First-principles study of defect-induced potentials in $Ca_2CuO_2Cl_2$

Yu Kumagai,[1] Fumiyasu Oba,[1,*] Ikuya Yamada,[2] Masaki Azuma,[3] and Isao Tanaka[1,4]
[1]*Department of Materials Science and Engineering, Kyoto University, Sakyo, Kyoto 606-8501, Japan*
[2]*Graduate School of Science and Engineering, Ehime University, Bunkyo-cho, Matsuyama, Ehime 790-8577, Japan*
[3]*Institute for Chemical Research, Kyoto University, Uji, Kyoto 611-0011, Japan*
[4]*Nanostructures Research Laboratory, Japan Fine Ceramics Center, Atsuta, Nagoya 456-8587, Japan*
(Received 17 March 2009; revised manuscript received 27 July 2009; published 27 August 2009)

The local atomic and electronic structures of the Na and K impurities and the vacancy at the Ca site (Na_{Ca}, K_{Ca}, and V_{Ca}), and their induced electrostatic potentials in $Ca_2CuO_2Cl_2$ have been investigated by using the GGA+U approach. It is found that Na_{Ca} and K_{Ca} are markedly relaxed toward the Cl plane from the original Ca site. When V_{Ca} exists, its neighboring Ca approaches the vacancy site, and Cl and O are relaxed outwardly. From the analyses of the local electrostatic potentials at the Cu and O sites, we found that the Na_{Ca}-induced potential is almost the same as the K_{Ca}-induced potential, and the V_{Ca}-induced potential is about twice as large. The defect-induced potentials are modeled by point charges under a dielectric medium. The atomic relaxation is found to increase the effective dielectric constants approximately threefold, indicating the importance of its contribution to the screening of the potential. The stabilization energies of small polarons obtained by the total energy differences are close to the potential energies. These results suggest that the interaction between the polaron and defects is well described by a positive charge of the polaron under the defect-induced electrostatic potential.

DOI: 10.1103/PhysRevB.80.085120 PACS number(s): 71.38.−k, 74.62.Dh, 74.72.−h

I. INTRODUCTION

Since the discovery of high-T_c superconductivity in Ba doped La_2CuO_4,[1] a considerable amount of research has been carried out to elucidate the mechanism of high-T_c superconductivity and to search for compounds with a higher T_c. Na-doped copper oxychloride, $Ca_{2-x}Na_xCuO_2Cl_2$, which exhibits superconductivity with T_c=28 K at a concentration of x =0.18, has attracted great interest due to its several advantages for studying the fundamental mechanism of high-T_c superconductivity.[2–8] The parent compound, $Ca_2CuO_2Cl_2$ (CCOC), has the same structure as K_2NiF_4-type La_2CuO_4. However, whereas La_2CuO_4 exhibits a transition from a high-temperature tetragonal ($I4/mmm$) phase to a low-temperature orthorhombic ($Abma$) phase at 520 K, CCOC maintains its undistorted tetragonal symmetry in the temperature range of 10–300 K.[9] Moreover, the single crystals of $Ca_{2-x}Na_xCuO_2Cl_2$ are very easily cleaved along the c plane. Their flat and clean surfaces are ideal for studies using surface-sensitive techniques such as scanning tunneling spectroscopy/microscopy (STS/STM) (Ref. 5–7) and angle-resolved photoemission spectroscopy (ARPES),[8] which can reveal the electronic structure in the real and reciprocal spaces, respectively.

The superconductivity occurs when a sufficient number of holes or electrons are introduced into an antiferromagnetic insulator with two-dimensional CuO_2 planes. In the case of CCOC, hole doping is conducted by substituting Ca with Na or K (Na_{Ca} and K_{Ca}), or by introducing Ca vacancies (V_{Ca}), leading to superconductivity with T_c=28,[3] 24,[10] and 43 K,[11] respectively. Such defects inevitably introduce defect-induced electrostatic potential. Recently, low-temperature STM measurements revealed spatially inhomogeneous electronic states in $Ca_{2-x}Na_xCuO_2Cl_2$.[5] Two scenarios have been proposed for the origin of the inhomogeneity: one is an electronic phase separation, and the other is a poorly screened Na-induced impurity potential. However, no conclusion has been drawn from the STM/STS measurements. Similar spatial inhomogeneity has also been observed in $Bi_2Sr_2CaCu_2O_y$.[12] In general, it is quite difficult to quantify the defect-induced potential from experiments. In this study, we evaluate the Na_{Ca}-, K_{Ca}-, and V_{Ca}-induced potentials in CCOC for low defect concentrations using first-principles calculations. The local atomic and electronic structures of the defects are also investigated.

The parent compound, CCOC, is known as a charge-transfer-type Mott insulator.[8] The conventional approximations to density-functional theory (DFT), such as the local spin-density approximation (LSDA), and generalized gradient approximation (GGA), fail to give the correct ground state for such systems. This is partly due to the spurious self-interaction in the LSDA and GGA, which has a tendency to delocalize electrons. In general, the error associated with self-interaction becomes large for localized orbitals. The LSDA predicts CCOC to be metallic and nonmagnetic, which disagrees with the insulating and antiferromagnetic state observed in experiments. On the other hand, the unrestricted Hartree-Fock method, which considers exchange interactions in an exact manner, qualitatively reproduces the antiferromagnetic insulating state.[13] However, the band gap and magnetic moment are significantly overestimated because of the exclusion of the correlation effects. To overcome the drawbacks of these approaches, the +U correction,[14,15] self-interaction correction (SIC),[16,17] and hybrid Hartree-Fock density functional[18–20] have been applied to cuprate systems in recent years. Although the +U correction and hybrid methods require system dependent parameters, i.e., the effective on-site Coulomb interaction and the amount of the Fock exchange, respectively, the electronic structure of metal oxides with valence or semicore 3d states can be well described by carefully choosing these

parameters.[20–26] In this study, we employed the $+U$ approach in conjunction with the GGA (GGA$+U$) to correct on-site Coulomb interactions of spatially localized Cu-3d electrons in CCOC. The $+U$ correction has an advantage in computational cost compared with the SIC and hybrid functional approaches. Because large supercells are required to evaluate the defect-induced potential for low defect concentrations, the $+U$ correction is the best choice for the purpose of our study.

This paper is organized as follows: after describing the computational procedures in Sec. II, we discuss the electronic and structural properties of perfect CCOC calculated using the GGA$+U$ in Sec. III A. The results of systems with a small polaron are then presented in Sec. III B. Recently, Patterson has reported that the B3LYP hybrid functional predicts a small polaron as the ground state in hole-doped CCOC at the low-hole-density limit.[26] Here, we give the spatial distribution and electronic structure of the small polaron calculated using the GGA$+U$ and the effect of the defects, namely, Na_{Ca}, K_{Ca}, and V_{Ca}, on the polaron. In Sec. III C, the local atomic and electronic structures around the defects and the defect-induced potentials in CCOC are discussed.

II. COMPUTATIONAL PROCEDURES

The calculations were performed using the projector augmented wave (PAW) method[27] as implemented in the VASP code.[28–30] The wave functions were expanded in a plane-wave basis set with an energy cutoff of 550 eV. We used the standard PAW potentials in the VASP distribution,[28] where Cu 3d, 4s, 4p; Ca 3p, 4s, 4p; Cl 3s, 3p; K 3p, 4s, 4p; Na 3s, 3p and O 2s, 2p electrons were described as valence electrons. The PAW radial cutoffs were 1.2, 1.6, 1.1, 1.7, 1.2, and 0.8 Å for Cu, Ca, Cl, K, Na, and O, respectively. The site-projected density of states (PDOS) and local magnetic moments were also evaluated within these spheres. Spin polarization was taken into account for all calculations. The exchange and correlation effects were treated within the GGA using the Perdew-Burke-Ernzerhof functional.[31] The strong on-site Coulomb interaction on Cu-3d orbitals was considered by the $+U$ correction (GGA$+U$). We adopted the simplified rotationally invariant formalism suggested by Dudarev *et al.*,[15] which is given as

$$E_{\mathrm{GGA}+U} = E_{\mathrm{GGA}} + \frac{U-J}{2}\sum_{\sigma}\left[\sum_{i}\rho_{ii}^{\sigma} - \sum_{i,j}\rho_{ij}^{\sigma}\rho_{ji}^{\sigma}\right], \qquad (1)$$

where E_{GGA} is the total energy evaluated using the GGA, U is the on-site Coulomb interaction parameter, J is the exchange interaction parameter, and ρ_{ij}^{σ} is the density matrix of the d electrons in spin state σ. In this formula, only the difference between U and J, $U'=U$-J, has a meaning. The reported values of U for the 3d orbitals of divalent Cu ions range between 4 and 8 eV, which were obtained using the constrained-density-functional method in a first-principles manner or by empirically fitting the band gaps.[32–36] In this study, we used three different values of U, namely, 7, 8, and 9 eV, and set J at 1 eV, which is a common value for 3d transition-metal compounds. This corresponds to $U'=6$, 7, and 8 eV.

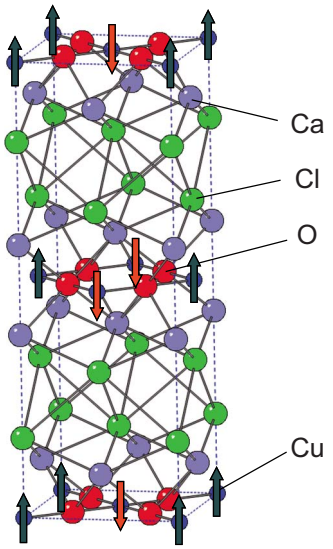

FIG. 1. (Color online) Crystal structure of CCOC. A $\sqrt{2}\times\sqrt{2}\times 1$ cell for describing the antiferromagnetic ordering at the Cu site is shown. The arrows denote spin directions.

Concerning hole-doped CCOC, Patterson has reported that a hole is localized as a small polaron in a $4\times4\times1$ CCOC supercell when the weight of the Fock exchange is set at 0.4 in the B3LYP hybrid functional.[26] As shown later, we found that the small polaron is also modeled using the GGA$+U$. We investigated the atomic and electronic structures of the polaron in CCOC both with and without a defect. In the case of perfect CCOC, the polaron is introduced by reducing the number of electrons by one. The number of small polarons in the defect systems is related to the formal defect charge. For instance, the neutral defects, Na_{Ca}^{0} and K_{Ca}^{0}, involve one polaron and V_{Ca}^{0} involves two polarons, where superscripts denote the charge states. To study the polaron, we considered these neutral defects and V_{Ca}^{-} (with one polaron). On the other hand, the polaron was excluded for the studies of the defect-induced potential so as to omit its screening effect. The defects investigated in this case are Na_{Ca}^{-}, K_{Ca}^{-}, and V_{Ca}^{2-}. The neutrality of the charged supercells was maintained by a compensating uniform background charge.

While the conventional unit cell composed of 14 atoms has only one Cu^{2+} ion in one CuO_2 plane, the $\sqrt{2}\times\sqrt{2}\times1$ supercell (Fig. 1) is needed to describe antiferromagnetic ordering in the CuO_2 planes. We used this cell to investigate perfect CCOC. A $3\sqrt{2}\times3\sqrt{2}\times1$ supercell containing 252 atoms was employed for the calculation of the systems with a small polaron and/or a defect. The defects, Na_{Ca}, K_{Ca}, and V_{Ca}, were introduced into one Ca site in the supercell, giving a defect concentration of 1.4%/Ca site. The k points were sampled in accordance with a Monkhorst-Pack scheme. A $4\times4\times2$ k mesh and the Γ point were used for the $\sqrt{2}\times\sqrt{2}\times1$ and $3\sqrt{2}\times3\sqrt{2}\times1$ supercells, respectively. For perfect CCOC, the lattice constants and internal coordinates were optimized until the residual stresses and forces converge to less than 0.05 GPa and 0.01 eV/Å, respectively. When we calculated the systems with a small polaron and/or a defect, only the internal coordinates were optimized and

TABLE I. Calculated indirect band gap (E_g), local magnetic moment on the Cu site (m_{Cu}), and energy difference between antiferromagnetic ordering and ferromagnetic ordering in $Ca_2CuO_2Cl_2$ (E_{AFM}-E_{FM}).

	U' (eV)	E_g (eV)	m_{Cu} (μ_B)	E_{AFM}-E_{FM} (meV/Cu^{2+})
LDA		0	0	
LDA+U	7	1.42	0.54	−167
GGA		0	0	
GGA+U	6	1.35	0.55	−159
	7	1.63	0.59	−175
	8	1.93	0.63	−153
Cal. (HF)[a]		16.8	0.92	−32
Cal. (B3LYP)[b],[c]		2.6[b]	0.60[c]	−160[b]

[a]Reference 13.
[b]Reference 20.
[c]Reference 26.

the lattice constants were fixed at those of the optimized values for perfect CCOC.

III. RESULTS AND DISCUSSION

A. Fundamental properties of perfect $Ca_2CuO_2Cl_2$

The calculated band gap, local magnetic moment on the Cu site, and energy difference between antiferromagnetic (AFM) ordering and ferromagnetic (FM) ordering per Cu^{2+} are listed in Table I. The structural properties are also summarized in Table II. The results of the LSDA (Ref. 16) and LSDA+U (U'=7 eV) calculations are shown as well as those using the GGA and GGA+U. It has been reported that the LSDA and GGA predict two-dimensional CuO_2 systems to be nonmagnetic metals in contrast to the observed antiferromagnetic insulators.[9] We have also identified the nonmagnetic metallic ground state in CCOC using the LSDA and GGA. It is generally considered that this qualitatively incorrect prediction is partly due to the spurious self-interaction in the LSDA and GGA. When the on-site Coulomb interactions of the Cu-3d orbitals are explicitly taken into account by the +U correction method, a band gap appears and the magnetic ordering of Cu is recovered. As U' increases, the Cu-3d orbitals become spatially localized and the magnetic moment slightly increases from 0.55 μ_B for U'=6 eV to 0.63 μ_B for U'=8 eV. All the +U calculations show that the AFM is energetically more favorable than the FM, as found in the previous reports using the B3LYP hybrid functional[18] and the unrestricted Hartree-Fock method.[12] The exchange interaction constant between the nearest neighbors, J_{NN}, in a spin-half system with a square lattice is extracted by mapping the total energies for the AFM and FM onto the Ising Hamiltonian,[13]

$$H_{spin} = -\sum_{\langle ij \rangle} J_{NN} S_i S_j, \tag{2}$$

where the summation for site i and j runs over the nearest neighbors, and a positive value of J_{NN} corresponds to ferromagnetic coupling. Using Eq. (2), J_{NN} is evaluated as J_{NN} =E_{AFM}-E_{FM}. The results for different U' values are listed in Table I. We found that J_{NN} is minimized at U'=7 eV when U' is shifted from 0 to 10 eV. For U' values of 6–8 eV, which are typical for cuprates, J_{NN} does not vary significantly (within 15%). The values of J_{NN} are close to the experimental values for two-dimensional CuO_2 systems (e.g., -166 ± 6 meV in La_2CuO_4)[37] and the theoretical value for CCOC obtained using the B3LYP hybrid functional (-160 meV).[20]

Figure 2 illustrates the calculated total density of states (DOS) and PDOS of perfect CCOC obtained using the GGA and GGA+U (U'=7 eV). The band structures are shown in Fig. 3. The valence-band top (VBT) in the GGA result is mainly composed of both Cu-3d and O-2p orbitals, which exhibit strong covalent interactions. The corresponding band is half filled as shown in Fig. 3, i.e., it exhibits a metallic

TABLE II. Calculated volume, lattice constants, internal structural parameters of Ca and Cl (z_{Ca} and z_{Cl}), and Cu-O bond length ($d_{Cu\text{-}O}$) in $Ca_2CuO_2Cl_2$. Calculated and experimental data in the literature are also listed.

	U' (eV)	V (Å^3)	a (Å)	c (Å)	z_{Ca}	z_{Cl}	$d_{Cu\text{-}O}$ (Å)
LDA		103.32	3.78	14.46	0.395	0.184	1.89
LDA+U	7	101.86	3.75	14.47	0.395	0.183	1.88
GGA		118.62	3.87	15.86	0.400	0.177	1.93
GGA+U	6	117.57	3.85	15.84	0.401	0.176	1.93
	7	117.29	3.85	15.83	0.401	0.176	1.93
	8	116.94	3.85	15.81	0.401	0.176	1.92
Cal. (HF)[a]		121.27	4.02	15.00	0.395	0.182	2.01
Cal. (B3LYP)[b]		117.57	3.94	15.12	0.396	0.185	1.97
Expt.[c]		112.6	3.87	15.05	0.396	0.183	1.93

[a]Reference 13.
[b]Reference 20.
[c]Reference 40.

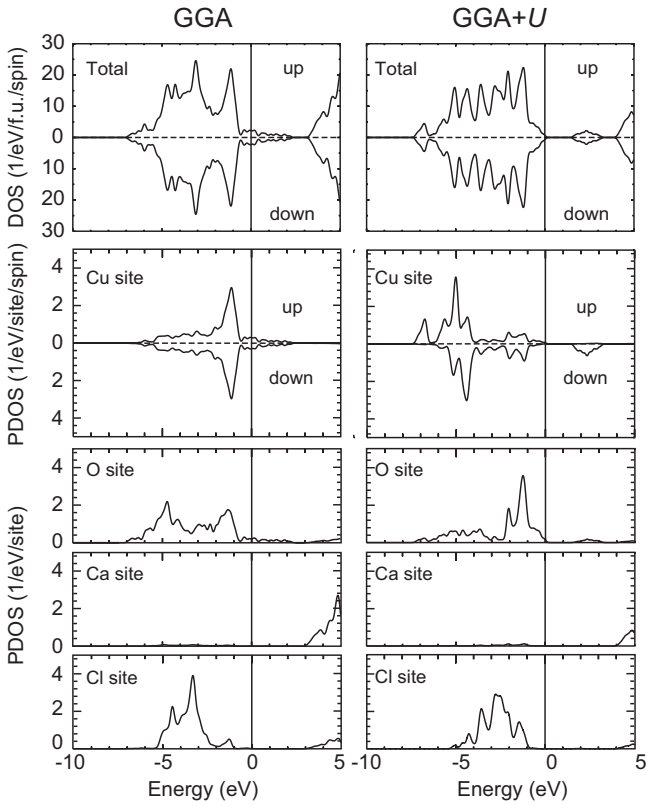

FIG. 2. Total and site-projected partial density of states of perfect CCOC obtained using the GGA and GGA+U ($U'=7$ eV). The zeros of the energy in the GGA and GGA+U results are placed at the Fermi level and the VBT, respectively.

characteristic. These DOS and band structures are very similar to those obtained by the local-density approximation.[38,39] When the on-site Coulomb interactions on the Cu-3d orbitals are considered, the electronic structure drastically changes. The VBT becomes mainly composed of the O-2p orbitals; this is a typical characteristic of a charge-transfer Mott insulator. The Cl-3p components are a few eV lower than the O-2p components, and make almost no contribution to the VBT. Opposite the GGA band structure, there is an indirect gap of 1.63 eV ($U'=7$ eV); the VBT and conduction band bottom (CBB) are located at points X and M, respectively. We found that the gap increases with increasing U' (e.g., 1.35 eV for $U'=6$ eV, and 1.93 eV for $U'=8$ eV). This is because the CBB is mainly composed of the Cu-3$d_{x^2-y^2}$ orbitals, which are directly affected by the on-site Coulomb interaction correction. Note, however, that the band structure is qualitatively preserved.

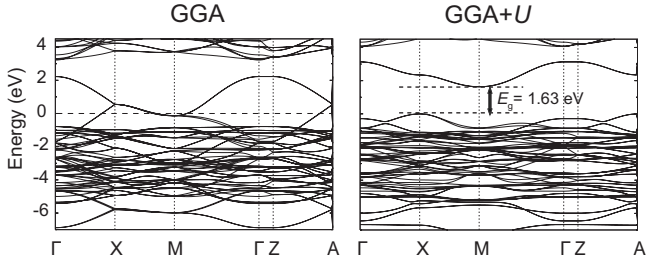

FIG. 3. Band structures of perfect CCOC obtained using the GGA and GGA+U ($U'=7$ eV). The zeros of the energy in the GGA and GGA+U results are placed at the Fermi level and the VBT, respectively. The symmetry points are based on the $\sqrt{2}\times\sqrt{2}\times 1$ tetragonal supercell.

Concerning the structural properties, the calculated volume obtained by the LSDA is 8% smaller and that obtained by the GGA is 5% larger than the experimental value. These are typical tendencies observed using the LSDA and GGA. The addition of U' to the GGA slightly decreases the volume, probably because of the localization of Cu-3d electrons. The overestimation of the lattice constant c by the GGA and GGA+U is mainly due to the overestimation of the interplanar distance between weakly bound Cl planes by 0.33 and 0.30 Å, respectively. The other structural properties calculated using the GGA and GGA+U, such as the other interplanar distance and the Cu-O bond length, are in excellent agreement with the experiment.

In summary, the atomic and electronic structures do not significantly depend on the value of U' when it is varied within typical values of 6–8 eV. Hereafter, we will show the results for $U'=7$ eV unless otherwise noted.

B. Small-polaron state

It is now widely accepted from both experimental[41–43] and theoretical viewpoints[44–48] that in high-T_c cuprate superconductors a hole in a low-hole-density region spatially localizes with a local lattice strain to form a small polaron. Because the VBT of high-T_c cuprate superconductors is composed of both Cu-3d and O-2p orbitals, the polaron exists in CuO_2 planes. The earlier theoretical studies have modeled the polaron state using model Hamiltonian.[44,45] The polaron state has also been described by first-principles methods. Recently, Patterson has reported that the B3LYP hybrid functional predicts a small polaron as the ground state in hole-doped CCOC at the low-density limit when the Fock exchange weight is suitably adjusted.[26] Anisimov *et al.*[48] have reported that the LSDA+U predicts the small-polaron state in La_2CuO_4. In this subsection, we show that the GGA+U also reproduces the small polaron as the stable state in CCOC. The electronic and magnetic structures of the polaron and the influences of the three defects, namely, Na_{Ca}, K_{Ca}, and V_{Ca}, on the polaron are also discussed.

When a hole is introduced into perfect CCOC, small-polaron and delocalized-hole states are obtained as stable and metastable states, respectively. The energy difference between these states is only 5 meV for $U'=7$ eV. However, as shown later, the small-polaron state becomes a few tenths eV more stable when the defects are introduced.

Figure 4(b) shows spin-density maps on the CuO_2 plane of perfect CCOC and that with a small polaron, and Fig. 4(c) shows the spatial distribution of the difference in charge density between the systems with and without a small polaron ($U'=7$ eV). It can be seen in Fig. 4(c) that the small polaron is mostly confined to one CuO_4 unit and is slightly distributed toward the nearest Cu and O sites. The Cu-O length in the CuO_4 unit is 0.04 Å (−2.1%) less than that in the unit without a polaron. The central Cu^{2+} ion in the small polaron

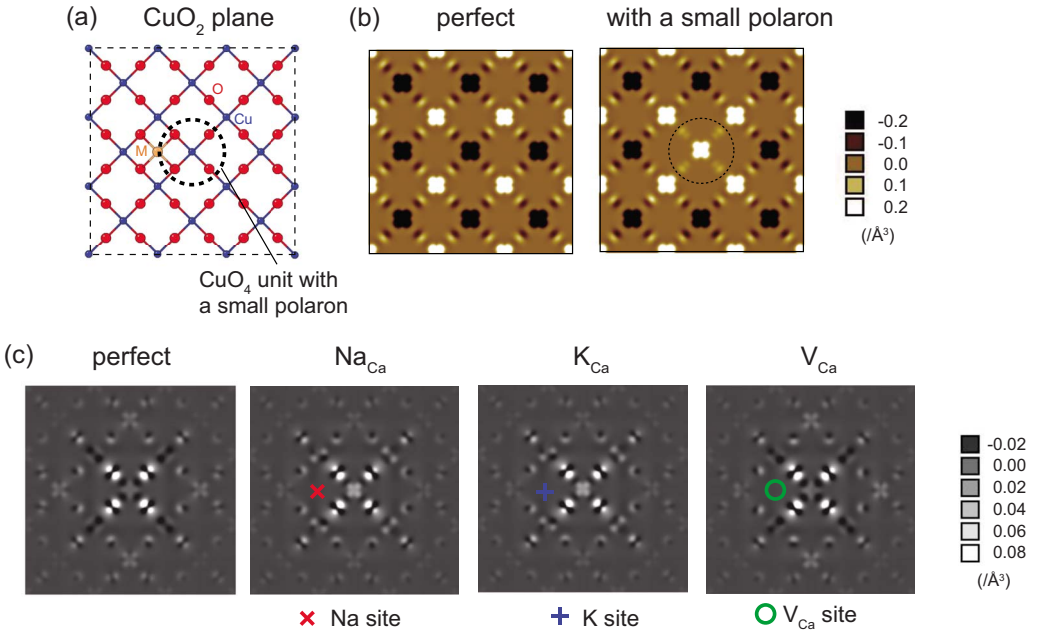

FIG. 4. (Color online) (a) Schematic of the CuO_2 plane. (b) Spin density maps on the CuO_2 plane of perfect CCOC and that with a small polaron. The dashed circle shows the CuO_4 unit containing a small polaron. (c) Charge density differences between the systems without (ρ_0) and with (ρ_1) a small polaron ($\Delta\rho=\rho_0-\rho_1$). The charge densities without a polaron were calculated using the same geometries as those with a polaron.

is ferromagnetically coupled with the nearest Cu^{2+} ions, breaking the antiferromagnetic ordering. Its magnetic moment is 0.42 μ_B ($U'=7$ eV), which is smaller than that for the Cu^{2+} ion in perfect CCOC by 0.17 μ_B. When U' is varied from 6 to 8 eV, the magnetic moment of the central Cu^{2+} ion changes from 0.31 to 0.59 μ_B, preserving its sign. The O^{2-} ions in the small polaron exhibit a slight magnetic moment of 0.02 μ_B ($U'=7$ eV) with the same sign as that for the central Cu^{2+} ion. The flip of the central Cu moment in the small polaron is consistent with the previous reports on CCOC using the B3LYP hybrid functional and on La_2CuO_4 using LSDA+U.[26,48]

The band structures for the $3\sqrt{2}\times3\sqrt{2}\times1$ supercells with a small polaron ($U'=7$ eV) are shown in Fig. 5. A small-polaron state in perfect CCOC is found in the up-spin state at 0.17 eV above the VBT. Orbital component analysis indicated that 16.4 and 31.6% of the wave function at the point Γ are projected to the central Cu site and the four surrounding O sites, respectively. This directly shows that the small polaron is mainly localized on the O sites in a CuO_4 unit. A flat unoccupied band in the down-spin state is also observed at 0.71 eV above the VBT. As shown in Sec. III A, the energy bands near the CBB are mainly composed of the Cu-$3d_{x^2-y^2}$ orbitals. When a polaron exists in a CuO_4 unit, the Coulomb repulsion should be locally reduced at the Cu site. The unoccupied Cu-$3d_{x^2-y^2}$ orbital is considered to be spatially localized there, which results in the formation of the deep level.

Next, we discuss the effect of the defects on the polaron. Because Na_{Ca}^-, K_{Ca}^-, and V_{Ca}^{2-} defects are negatively charged, they are expected to stabilize a polaron that has a positive charge. Indeed, we found that this is energetically favorable when the polaron is located in the immediate vicinity of the defects. In this case, the spatial distributions of the polaron are slightly affected by the defects as shown in Fig. 4(c). The fractions projected on the Cu site (O sites) increase from 16.4 (31.6)% to 19.7 (34.2), 19.1 (33.8), and 20.5 (34.8)% for Na_{Ca}, K_{Ca}, and V_{Ca}, respectively. The magnetic moment of the central Cu site is reduced from 0.42 μ_B to 0.34, 0.35, and 0.32 μ_B, respectively. These changes indicate that the

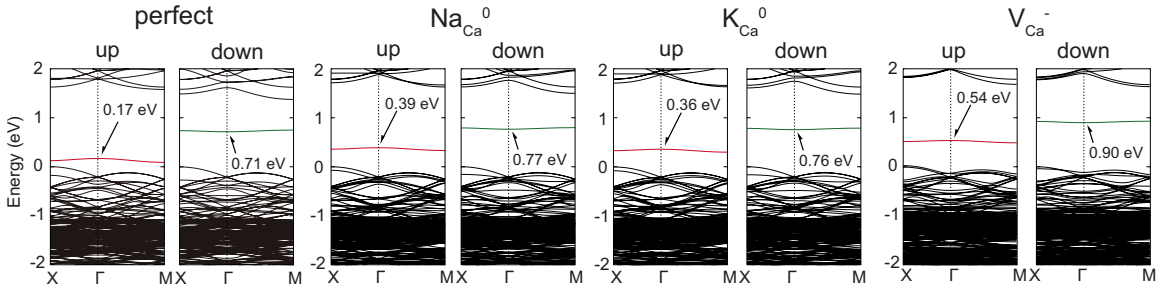

FIG. 5. (Color online) Calculated band structures for perfect and defective supercells with a small polaron. The zeros of energy are placed at the VBT. The arrows indicate the bands associated with the polaron. Their energies with respect to the VBT are also shown.

defects have a tendency to spatially localize the polaron. As shown in Fig. 5, when the defects exist, the energy bands associated with a polaron become 0.22, 0.19, and 0.37 eV higher than that in perfect CCOC, respectively. The Cu-O length next to the dopant in the CuO_4 unit is slightly shorter than that on the other side of the unit by 0.03 Å.

We also calculated the small-polaron stabilization energy (E_s) for Na_{Ca} and K_{Ca}, i.e., the binding energy between the polaron and defects, as

$$E_s = [E_d^0(M) - E_d^-(M)] - [E_p^+ - E_p^0], \tag{3}$$

where E_p^q and $E_d^q(M)$, respectively, denote the total energies of the perfect CCOC supercell and the supercell containing a defect M_{Ca} (M=Na or K) (M_{Ca}-CCOC) with charge q. The energy references for the charged supercells were aligned with that for the neutral perfect CCOC supercell via alignments of the average electrostatic potential at the outermost Cu site from a small polaron or a defect with that in perfect CCOC.[49,50] The calculated E_s for Na_{Ca} and K_{Ca} are −0.25 and −0.24 eV, respectively. In the next subsection, we compare these values with the potential energies for a small polaron estimated from the defect-induced electrostatic potential.

C. Local atomic structures and defect-induced potentials

Figure 6 shows the relaxed structures around Na_{Ca}^-, K_{Ca}^-, and V_{Ca}^{2-} in CCOC without a polaron alongside that around Ca in perfect CCOC (U'=7 eV). In spite of the fact that the ionic radius of Na^+, 1.16 Å, is almost the same as that of Ca^{2+}, 1.14 Å,[51] the equilibrium position of Na^+ is 0.20 Å away from the original Ca^{2+} site. The resultant Na-O length is 0.25 Å larger than the Ca-O length (2.48 Å) in perfect CCOC. This may be due to the weaker attractive electrostatic interaction between Na^+ and O^{2-} compared with that between Ca^{2+} and O^{2-}. The K-O length is much larger (2.95 Å) as expected from the large K^+ ionic radius (1.52 Å).[51] When V_{Ca}^{2-} exists, its neighboring Ca is relaxed inwardly by 0.32 Å, while Cl and O exhibit outward relaxations of 0.15 and 0.20 Å, respectively. These behaviors are attributed to the attractive and repulsive electrostatic interactions, respectively. We have also investigated the effects of the polaron on the local structures. When a small polaron is trapped, the local structures around the defects slightly change, as mentioned for the Cu-O length in Sec. III B. In particular, the distance between Ca and the defect, denoted as d' in Fig. 6, significantly increases by 0.11, 0.04, and 0.06 Å for Na_{Ca}, K_{Ca}, and V_{Ca}, respectively. This may be due to the electrostatic repulsion between the polaron and cations.

To investigate the effects of the Na_{Ca}^-- and V_{Ca}^{2-}-induced potentials on the electronic structure, we calculated the O-2p PDOS, which mainly constitutes the VBT. The defects without a polaron are considered here in order to omit its screening effect. In Fig. 7, the O-2p PDOS at the first nearest neighbor (1NN), the second nearest neighbor (2NN), and the farthest O sites from the defect in the $3\sqrt{2}\times 3\sqrt{2}\times 1$ supercells are shown along with that of perfect CCOC. The PDOS without and with atomic relaxation are compared so as to elucidate the effects of atomic relaxation on the screening of

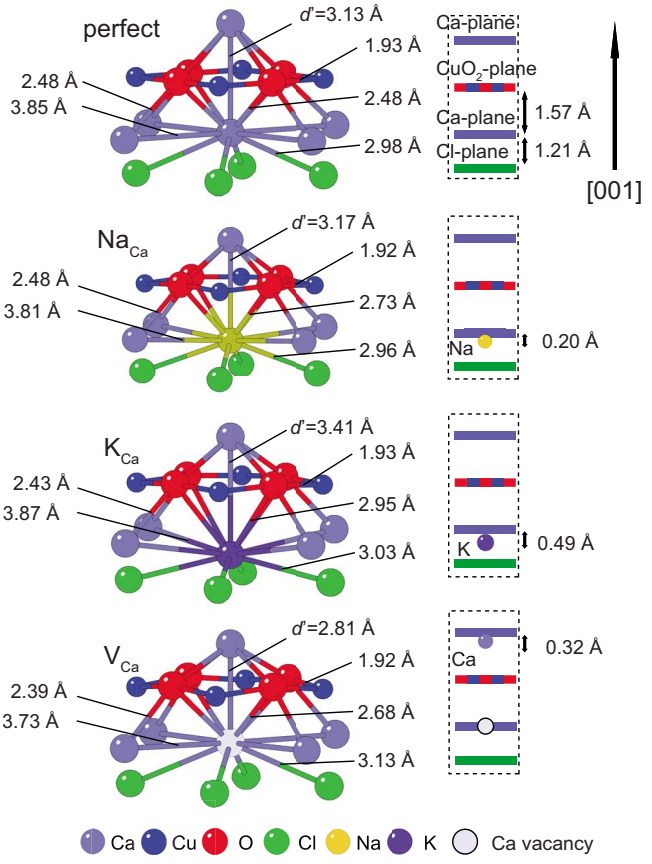

FIG. 6. (Color online) Local atomic structures around Na_{Ca}^-, K_{Ca}^-, and V_{Ca}^{2-} in $Ca_2CuO_2Cl_2$ together with that around Ca in perfect $Ca_2CuO_2Cl_2$.

the defect-induced potential. In all cases, the PDOS at the farthest O site is almost identical with that in perfect CCOC, which indicates that the defect-induced potential is well screened there. Without taking the atomic relaxation into account, the dispersion of the PDOS at the 1NN site markedly differs from that for perfect CCOC and it exhibits large peaks near the VBT. An important finding is that when the atomic relaxation is taken into account, the shape of the PDOS at the 1NN site is nearly recovered to that in perfect CCOC, apart from a rigid shift of the PDOS by 0.4 and 0.5 eV owing to the Na_{Ca}^-- and V_{Ca}^{2-}-induced electrostatic potentials, respectively.

To discuss the defect-induced potentials quantitatively, we then evaluated the on-site electrostatic potential at 10 different Cu sites and 12 O sites in the $3\sqrt{2}\times 3\sqrt{2}\times 1$ supercells. Figure 8 shows the calculated relative average potential plotted against the inverse of the distance from the defect. Again, the defects without a polaron are considered. Since the formal charge of the V_{Ca}^{2-} defect is −2, the V_{Ca}^{2-}-induced potential would not be sufficiently screened by trapping only one polaron. Therefore, we also calculated the electrostatic potential of V_{Ca}^-, where a polaron is trapped by V_{Ca}^{2-}. To evaluate the potential, a test charge of +e was placed in spheres with radii of 1.01 and 0.72 Å for the Cu and O sites, respectively. The potential-energy differences from perfect CCOC are obtained for the Cu and O sites, and these are plotted in Fig. 8.

As expected from their formal charges, all the defects generate negative potentials for the +e test charge, and hence

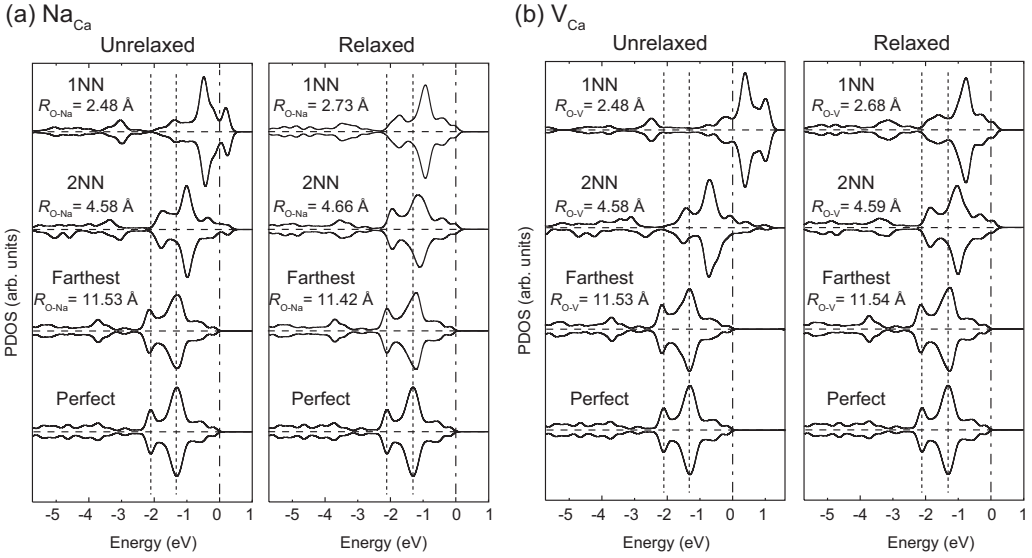

FIG. 7. O-2*p* PDOS at the 1NN, 2NN, and farthest O sites from the defects in the $3\sqrt{2}\times 3\sqrt{2}\times 1$ supercell along with that of perfect CCOC for structures without and with atomic relaxation: (a) Na_{Ca}^{-} and (b) V_{Ca}^{2-}. For the estimations of the distance from the defect, the V_{Ca} site is assumed to be the Ca site in perfect CCOC. The VBT at the farthest site is aligned with that in perfect CCOC. The broken lines are guides for eyes.

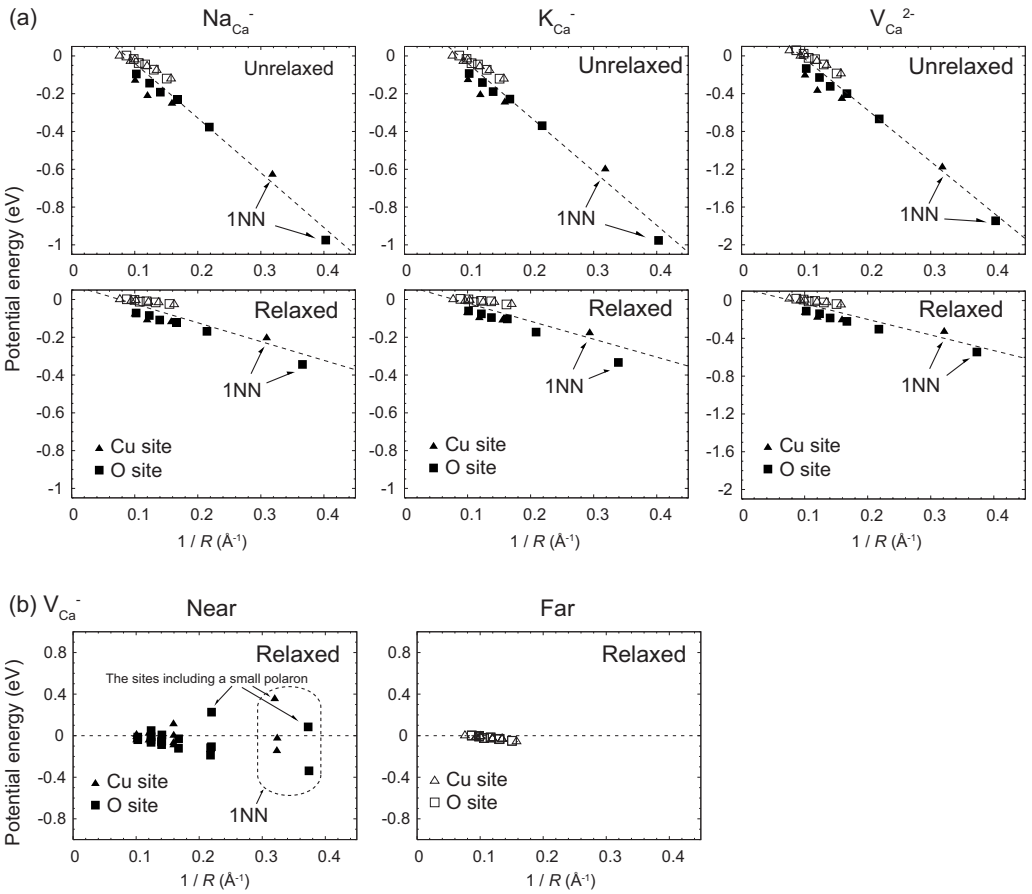

FIG. 8. Relative potential energies on the Cu and O sites for $+e$ charge in structures without and with atomic relaxation against the inverse of the distance from the defect. The V_{Ca} site is assumed to be the Ca site in perfect CCOC. Filled and open symbols denote values in the CuO_2 planes near and far from the defects, respectively. (a) The potential energies for Na_{Ca}^{-}, K_{Ca}^{-}, and V_{Ca}^{2-} (without a polaron). The broken lines are linear fits. (b) The potential energy for V_{Ca}^{-} (with one polaron). The zeros of the potential were placed at the outermost Cu site from the defects.

TABLE III. Calculated effective dielectric constants around the defects.

Defect	ε_∞	ε_0
Na_{Ca}	5.0	14.5
K_{Ca}	5.0	15.2
V_{Ca}	5.3	17.5

for the polaron. The Na_{Ca}^{-}-induced potential is almost the same as the K_{Ca}^{-}-induced potential, and the V_{Ca}^{2-}-induced potential is about twice as large. The potential is systematically lower in the CuO_2 plane located near the defects than that far from the defects, which suggests that the screening by the Ca and Cl planes is much larger than that within the CuO_2 planes. In all the cases, the defect-induced potential almost linearly depends on the inverse of the distance from the defect site, indicating the dominance of the monopolelike behavior. Therefore, the defect-induced potential can be modeled as $q/\varepsilon R$, where q is the defect charge ($q=-1$ for Na_{Ca} and K_{Ca}, and $q=-2$ for V_{Ca}), ε is the effective dielectric constant, and R is the distance from the defect. The effective dielectric constants obtained by fitting to this model are shown in Table III. The electronic and static dielectric constants (ε_∞ and ε_0) were obtained using the results without and with atomic relaxation, respectively. When finite-sized supercells are used to calculate the defect-induced potentials, the spurious image charge potential is caused by the repeated defects under three-dimensional periodic boundary conditions. One can estimate the potential by calculating the sum of the screened electrostatic potentials generated by the point charges located outside of the supercell under consideration. In the case of the result for relaxed Na_{Ca}, the error was found to be largest at the outermost Cu site. However, it was only a few tens of meV. This does not essentially affect the results presented in Fig. 8 and Table III. We have also verified that the effects of the spurious image charge potentials in other systems are also small.

For all the defects, the atomic relaxation strongly screens the defect-induced potential and increases the effective dielectric constants approximately threefold, i.e., $\varepsilon_0 \approx 3\varepsilon_\infty$. In the case of V_{Ca}^{-}, where a polaron is trapped, the potential energies on the sites in the CuO_4 unit including the polaron are increased from the value for V_{Ca}^{2-} because of the positive electrostatic potential caused by the polaron. The large variation in the potential with respect to the atomic sites is thought to be due to the electric dipole generated by the polaron and V_{Ca}^{2-}. The potential at the sites far from the polaron and V_{Ca} is similar to that of Na_{Ca} and K_{Ca}.

The polaron stabilization energy may be estimated by the potential-energy differences between a polaron near the defect and one at an infinite distance. Assuming that a small polaron is confined in a CuO_4 unit with the distribution of Cu:O=1:2, based on the orbital component analysis of the small polaron in perfect CCOC (Sec. III B), the potential energy for a small polaron at the nearest CuO_4 unit to the defect is estimated to be −0.25 and −0.24 for Na_{Ca} and K_{Ca}, respectively. These values are within 0.01 eV of those for E_s obtained in Sec. III B. Thus, the interaction between the small polaron and defects is well described by a positive charge of the polaron under the defect-induced electrostatic potential. This also indicates that the spatial distribution of the polaron and the atomic relaxation energy required for the creation of the polaron are similar for positions close to and far from the defects.

IV. SUMMARY

We have performed first-principles calculations using the GGA+U approach to investigate the local atomic and electronic structures around three defects, namely, Na_{Ca}, K_{Ca}, and V_{Ca}, and their induced electrostatic potentials in CCOC. In Sec. III A, the calculated electronic, magnetic, and structural properties of CCOC are discussed. The DOS and band structure exhibit a characteristic of an antiferromagnetic charge-transfer Mott insulator. The optimized crystal structures agree well with the experimental values except for the overestimation of the interplanar distance between the Cl planes. In Sec. III B, we give the spatial distribution and electronic states of a small polaron in CCOC. The small polaron is mainly localized on the O sites in a CuO_4 unit. Na_{Ca}, K_{Ca}, and V_{Ca} stabilize the polaron; these defects raise the one-electron state associated with the polaron by 0.22, 0.19, and 0.37 eV from that in perfect CCOC, respectively. In Sec. III C, the local atomic structures around the defects and the defect-induced potentials are discussed. It is found that Na_{Ca} and K_{Ca} are markedly relaxed toward the Cl plane from the original Ca^{2+} site. When V_{Ca} exists, its neighboring Ca approaches the vacancy site, and Cl and O are relaxed outwardly. From the analyses of the local electrostatic potentials at the Cu and O sites, we found that the Na_{Ca}^{-}-induced potential is almost the same as the K_{Ca}^{-}-induced potential, and the V_{Ca}^{2-}-induced potential is about two times larger. The defect-induced potentials were modeled by point charges with corresponding formal charges under a dielectric medium. The resultant dielectric constants are $\varepsilon_\infty=5.0-5.3$ and $\varepsilon_0=14.5-17.5$. ε_0 is about three times larger than ε_∞, indicating the importance of the effect of atomic relaxation on the screening. The calculated polaron stabilization energies for Na_{Ca} and K_{Ca} are −0.25 and −0.24 eV, respectively, which are close to the electrostatic potential energies. Thus, the interaction between the small polaron and defects is well described by a positive charge of the polaron under the defect-induced electrostatic potential.

ACKNOWLEDGMENTS

This work was supported by Grants-in-Aid for Scientific Research (A) and Priority Areas "Atomic Scale Modification" (No. 474), and the global COE program, all from the Ministry of Education, Culture, Sports, Science and Technology (MEXT) of Japan. Y.K. thanks the Japan Society for the Promotion of Science (JSPS).

*Author to whom correspondence should be addressed; oba@cms.mtl.kyoto-u.ac.jp

[1] J. B. Bednorz and K. A. Müller, Z. Phys. B **64**, 189 (1986).
[2] Z. Hiroi, N. Kobayashi, and M. Takano, Nature (London) **371**, 139 (1994).
[3] Z. Hiroi, N. Kobayashi, and M. Takano, Physica C **266**, 191 (1996).
[4] Y. Kohsaka, M. Azuma, I. Yamada, T. Sasagawa, T. Hanaguri, M. Takano, and H. Takagi, J. Am. Chem. Soc. **124**, 12275 (2002).
[5] Y. Kohsaka, K. Iwaya, S. Satow, T. Hanaguri, M. Azuma, M. Takano, and H. Takagi, Phys. Rev. Lett. **93**, 097004 (2004).
[6] T. Hanaguri, C. Lupien, Y. Kohsaka, D.-H. Lee, M. Azuma, M. Takano, H. Takagi, and J. C. Davis, Nature (London) **430**, 1001 (2004).
[7] T. Hanaguri, Y. Kohsaka, J. C. Davis, C. Lupien, I. Yamada, M. Azuma, M. Takano, K. Ohishi, M. Ono, and H. Takagi, Nat. Phys. **3**, 865 (2007).
[8] F. Ronning, T. Sasagawa, Y. Kohsaka, K. M. Shen, A. Damascelli, C. Kim, T. Yoshida, N. P. Armitage, D. H. Lu, D. L. Feng, L. L. Miller, H. Takagi, and Z.-X. Shen, Phys. Rev. B **67**, 165101 (2003).
[9] D. Vaknin, L. L. Miller, and J. L. Zarestky, Phys. Rev. B **56**, 8351 (1997).
[10] T. Tatsuki, S. Adachi, M. Itoh, T. Tamura, X.-J. Wu, C.-Q. Jin, N. Koshizuka, and K. Tanabe, Physica C **255**, 61 (1995).
[11] I. Yamada, A. A. Belik, M. Azuma, S. Harjo, T. Kamiyama, Y. Shimakawa, and M. Takano, Phys. Rev. B **72**, 224503 (2005).
[12] S. H. Pan, J. P. O'Neal, R. L. Badzey, C. Chamon, H. Ding, J. R. Engelbrecht, Z. Wang, H. Eisaki, S. Uchida, A. K. Gupta, K.-W. Ng, E. W. Hudson, K. M. Lang, and J. C. Davis, Nature (London) **413**, 282 (2001).
[13] I. de P. R. Moreira and R. Dovesi, Phys. Rev. B **67**, 134513 (2003).
[14] V. I. Anisimov, J. Zaanen, and O. K. Andersen, Phys. Rev. B **44**, 943 (1991).
[15] S. L. Dudarev, G. A. Botton, S. Y. Savrasov, C. J. Humphreys, and A. P. Sutton, Phys. Rev. B **57**, 1505 (1998).
[16] J. P. Perdew and A. Zunger, Phys. Rev. B **23**, 5048 (1981).
[17] W. M. Temmerman, H. Winter, Z. Szotek, and A. Svane, Phys. Rev. Lett. **86**, 2435 (2001).
[18] J. K. Perry, J. Tahir-Kheli, and W. A. Goddard III, Phys. Rev. B **63**, 144510 (2001).
[19] A. D. Becke, J. Chem. Phys. **98**, 5648 (1993).
[20] C. H. Patterson, Phys. Rev. B **77**, 115111 (2008).
[21] F. Oba, A. Togo, I. Tanaka, J. Paier, and G. Kresse, Phys. Rev. B **77**, 245202 (2008).
[22] C. Franchini, R. Podloucky, J. Paier, M. Marsman, and G. Kresse, Phys. Rev. B **75**, 195128 (2007).
[23] A. Walsh, J. L. F. Da Silva, and S.-H. Wei, Phys. Rev. Lett. **100**, 256401 (2008).
[24] A. Janotti, D. Segev, and C. G. Van de Walle, Phys. Rev. B **74**, 045202 (2006).
[25] S. Lany and A. Zunger, Phys. Rev. B **72**, 035215 (2005).
[26] C. H. Patterson, Phys. Rev. B **77**, 094523 (2008).
[27] P. E. Blöchl, Phys. Rev. B **50**, 17953 (1994).
[28] G. Kresse and D. Joubert, Phys. Rev. B **59**, 1758 (1999).
[29] G. Kresse and J. Furthmüller, Phys. Rev. B **54**, 11169 (1996).
[30] G. Kresse and J. Hafner, Phys. Rev. B **48**, 13115 (1993).
[31] J. P. Perdew, K. Burke, and M. Ernzerhof, Phys. Rev. Lett. **77**, 3865 (1996).
[32] V. I. Anisimov, M. A. Korotin, A. S. Mylnikova, A. V. Kozhevnikov, D. M. Korotin, and J. Lorenzana, Phys. Rev. B **70**, 172501 (2004).
[33] P. Blaha, K. Schwarz, and P. Novák, Int. J. Quantum Chem. **101**, 550 (2005).
[34] D. Wu, Q. Zhang, and M. Tao, Phys. Rev. B **73**, 235206 (2006).
[35] O. Le Bacq, A. Pasturel, C. Lacroix, and M. D. Núñez-Regueiro, Phys. Rev. B **71**, 014432 (2005).
[36] D. J. Singh and W. E. Pickett, Phys. Rev. B **44**, 7715 (1991).
[37] D. K. Morr, Phys. Rev. B **58**, R587 (1998).
[38] L. F. Mattheiss, Phys. Rev. B **42**, 354 (1990).
[39] D. L. Novikov, A. J. Freeman, and J. D. Jorgensen, Phys. Rev. B **51**, 6675 (1995).
[40] D. N. Argyriou, J. D. Jorgensen, R. L. Hitterman, Z. Hiroi, N. Kobayashi, and M. Takano, Phys. Rev. B **51**, 8434 (1995).
[41] K. M. Shen, F. Ronning, W. Meevasana, D. H. Lu, N. J. C. Ingle, F. Baumberger, W. S. Lee, L. L. Miller, Y. Kohsaka, M. Azuma, M. Takano, H. Takagi, and Z.-X. Shen, Phys. Rev. B **75**, 075115 (2007).
[42] G. Zhao, M. B. Hunt, H. Keller, and K. A. Müller, Nature (London) **385**, 236 (1997).
[43] X. X. Bi and P. C. Eklund, Phys. Rev. Lett. **70**, 2625 (1993).
[44] F. C. Zhang and T. M. Rice, Phys. Rev. B **37**, 3759 (1988).
[45] V. J. Emery and G. Reiter, Phys. Rev. B **38**, 4547 (1988).
[46] L. Hozoi, S. Nishimoto, G. Kalosakas, D. B. Bodea, and S. Burdin, Phys. Rev. B **75**, 024517 (2007).
[47] J. P. Hague, P. E. Kornilovitch, and A. S. Alexandrov, Phys. Rev. B **78**, 092302 (2008).
[48] V. I. Anisimov, M. A. Korotin, J. Zaanen, and O. K. Andersen, Phys. Rev. Lett. **68**, 345 (1992).
[49] T. Mattila and A. Zunger, Phys. Rev. B **58**, 1367 (1998).
[50] M. Choi, F. Oba, and I. Tanaka, Phys. Rev. B **78**, 014115 (2008).
[51] R. D. Shannon, Acta Crystallogr. A **32**, 751 (1976).